JGR Space Physics

RESEARCH ARTICLE
10.1029/2024JA032848

Equatorial Source of Oblique Electromagnetic Ion Cyclotron Waves: Peculiarities in the Ion Distribution Function

David S. Tonoian[1], Xiao-Jia Zhang[1,2], Anton Artemyev[2], and Xin An[2]

[1]Department of Physics, University of Texas at Dallas, Richardson, TX, USA, [2]Department of Earth, Planetary, and Space Sciences, University of California, Los Angeles, CA, USA

Key Points:

- We report observations of very oblique electromagnetic ion cyclotron (EMIC) waves around their equatorial source region
- Oblique EMIC wave generation is associated with field-aligned thermal ion streams and hot, transversely anisotropic ions
- The presence of field-aligned thermal ion streams attributes oblique EMIC wave generation to its possible ionospheric source

Correspondence to:
D. S. Tonoian,
david.tonoian@utdallas.edu

Citation:
Tonoian, D. S., Zhang, X.-J., Artemyev, A., & An, X. (2024). Equatorial source of oblique electromagnetic ion cyclotron waves: Peculiarities in the ion distribution function. *Journal of Geophysical Research: Space Physics*, *129*, e2024JA032848. https://doi.org/10.1029/2024JA032848

Received 1 MAY 2024
Accepted 5 NOV 2024

Author Contributions:
Conceptualization: Anton Artemyev
Data curation: Xiao-Jia Zhang, Xin An
Investigation: David S. Tonoian
Methodology: Xiao-Jia Zhang, Anton Artemyev, Xin An
Software: David S. Tonoian
Supervision: Xiao-Jia Zhang
Validation: Xiao-Jia Zhang, Xin An
Writing – original draft: David S. Tonoian
Writing – review & editing: Xiao-Jia Zhang, Anton Artemyev, Xin An

Abstract Electromagnetic ion cyclotron (EMIC) waves are important for Earth's inner magnetosphere as they can effectively drive relativistic electron losses to the atmosphere and energetic (ring current) ion scattering and isotropization. EMIC waves are generated by transversely anisotropic ion populations around the equatorial source region, and for typical magnetospheric conditions this almost always produces field-aligned waves. For many specific occasions, however, oblique EMIC waves are observed, and such obliquity has been commonly attributed to the wave off-equatorial propagation in curved dipole magnetic fields. In this study, we report that very oblique EMIC waves can be directly generated at the equatorial source region. Using THEMIS spacecraft observations at the dawn flank, we show that such oblique wave generation is possible in the presence of a field-aligned thermal ion population, likely of ionospheric origin, which can reduce Landau damping of oblique EMIC waves and cyclotron generation of field-aligned waves. This generation mechanism underlines the importance of magnetosphere-ionosphere coupling processes in controlling wave characteristics in the inner magnetosphere.

1. Introduction

Electromagnetic ion cyclotron (EMIC) waves are a natural emission generated by transversely anisotropic ion (proton) populations in the Earth's inner magnetosphere (Cornwall et al., 1970; Cornwall & Schulz, 1971; Min et al., 2015; Yue et al., 2019). These waves are responsible for resonant scattering of relativistic electrons and energetic (ring current) ions (see review Usanova et al., 2016, and references therein), which makes this wave mode principally important for the inner magnetosphere dynamics.

Transversely anisotropic ion populations, either injected from the plasma sheet or formed due to the magnetosphere compression by solar wind transients (Jun et al., 2019, 2021; Kim et al., 2021), usually generate field-aligned EMIC waves (Chen et al., 2010, 2011), whereas generation of oblique waves is often suppressed by wave Landau damping due to thermal ions (see discussions in de Soria-Santacruz et al., 2013). Thus, oblique EMIC waves have been mostly detected off the equator (Liu et al., 2013), because wave propagation in highly inhomogeneous magnetic field and plasma will result in wavevector deviation from the field-aligned direction (Fraser & Nguyen, 2001; Rauch & Roux, 1982; Thorne & Horne, 1997). It has been shown that oblique EMIC waves can scatter particles via several resonant mechanisms not available to field-aligned waves (see review by Usanova, 2021). First, wave obliquity modifies the efficiency of relativistic electron scattering (see Hanzelka et al., 2023; Khazanov & Gamayunov, 2007; Lee et al., 2018). Second, the Landau resonance between oblique EMIC waves and cold ions allows EMIC waves to mediate the energy transfer between hot and cold ion populations (Kitamura et al., 2018; Ma et al., 2019; Omura et al., 1985). Third, oblique EMIC waves can resonate with cold plasmasphere electrons (in linear and nonlinear regimes, see B. Wang et al., 2019) and can accelerate and/or precipitate them to form the stable red aurora arcs (Cornwall et al., 1971; Thorne & Horne, 1992). Fourth, oblique EMIC waves may scatter energetic ($\sim$100 keV) electrons via the bounce resonance (Q. Wang et al., 2018; Blum et al., 2019). All these mechanisms imply the importance of understanding possible sources of oblique EMIC waves: can such waves be generated around the equator or only off-equator as the field-aligned waves propagate away from their equatorial source?

The equatorial generation of oblique EMIC waves requires a viable mechanism to suppress the Landau damping, that is, reduction of the field-aligned gradient in the ion phase space density around the Landau resonant energies (hundreds of eV). For the electron-scale whistler-mode waves, it has been shown that oblique wave generation can be explained by field-aligned electron streams generated by ionosphere outflow (see discussions in Artemyev & Mourenas, 2020), which largely suppress Landau damping (see, e.g., Mourenas et al., 2015; Li et al., 2016).

Such ionosphere outflows also include field-aligned ionospheric ion populations, which are often detected in the inner magnetosphere and near-Earth plasma sheet (Artemyev et al., 2018; Yue et al., 2017). Therefore, oblique EMIC wave generation may be explained by a combination of near-equatorial, transversely anisotropic hot ions and field-aligned thermal ion streams.

In this study, we investigate near-equatorial observations of very oblique EMIC waves by Time History of Events and Macroscale Interactions during Substorms (THEMIS) spacecraft (Angelopoulos, 2008). Combining measurements of ion distribution functions (McFadden et al., 2008) and linear dispersion solver (Astfalk & Jenko, 2017), we reveal the conditions of such wave generation and demonstrate that very oblique EMIC waves are associated with field-aligned ion streams. The rest of this paper is structured as follows: Section 2 describes THEMIS instrumentation, plasma and wave measurements, methods of data analysis, and details of the linear dispersion solver. Section 3 examines the generation of very oblique EMIC wave in multiple events by analyzing the observed ion distribution functions and comparing these distributions with that during field-aligned EMIC waves. Section 4 summarizes our results and discusses their implication for modeling particle dynamics in the inner magnetosphere.

2. Data Set and Instruments

We combine near-equatorial THEMIS measurements of EMIC waves (of 16 Hz sampling rate from the flux-gate magnetometer, see Auster et al., 2008), plasma sheet ion distributions (at 3 s resolution from the electrostatic analyzer (ESA), covering <25 keV energy range and full pitch-angle range, see McFadden et al., 2008), total plasma density inferred from the spacecraft potential (see Bonnell et al., 2008; Nishimura et al., 2013), and the numerical dispersion solver for electromagnetic waves—Linear Electromagnetic Oscillations in Plasmas with Arbitrary Rotationally symmetric Distributions (LEOPARD, see Astfalk & Jenko, 2017). Because ESA cannot separate different ion species, we assume that the ion population is dominated by protons. We also compare ion and electron densities to confirm this assumption (see details in Artemyev et al., 2020). We use the single-spacecraft maximum variance analysis technique (Means, 1972) to estimate the wave normal angle, which comes with an ambiguity of parallel versus anti-parallel directions: the wave normal angle from this technique ranges from 0° to 90°, rather than 0° to 180°.

An important advantage of LEOPARD model is it accommodates arbitrary gyrotropic distribution functions in a uniform grid of velocities parallel and perpendicular to the background magnetic field, $(v_{\parallel}, v_{\perp})$. Compared to dispersion solvers that require fitting the measurements to prescribed particle distributions (such as Maxwellians), LEOPARD significantly reduces the uncertainties due to fitting and hence can give a more reliable dispersion solution. Therefore, we use ESA ion distributions in 23 logarithmically spaced energy channels between 5 and 25 keV and 8 linearly spaced pitch-angle channels and interpolate them to a denser $(v_{\parallel}, v_{\perp})$ grid, which is then passed to LEOPARD as the proton distribution to evaluate the observed EMIC wave dispersion and growth rate. We will combine LEOPARD and THEMIS measurements to reveal properties of specific ion distributions that are responsible for the generation of very oblique EMIC waves. Note that although THEMIS ESA provides plasma sheet (<30 keV) electron distributions, this electron population usually does not resonate with EMIC waves or alter the wave dispersion. Thus, we only treat electrons as the cold background plasma (with electron $\beta = 10^{-2}$) and do not examine their contribution to EMIC wave growth.

3. Oblique EMIC Events

We now analyze in details multiple events with very oblique EMIC waves. These are typical events of this wave population and hence their characteristics will be representative of the entire population.

3.1. Detailed Analysis of the First Event

The first event shows very oblique EMIC waves observed by THEMIS-A spacecraft on 17 February 2020, between 17:50–17:58 UT (Figure 1). During this event, hydrogen-band EMIC waves (of frequencies within $0.3 - 0.9$ of the proton cyclotron frequency f_{cH+}) were detected in the dawn flank of the outer edge of the inner magnetosphere (MLT $\sim$ 07, $L \sim 10$) with the presence of hot, plasma sheet ions. The EMIC wave normal angle

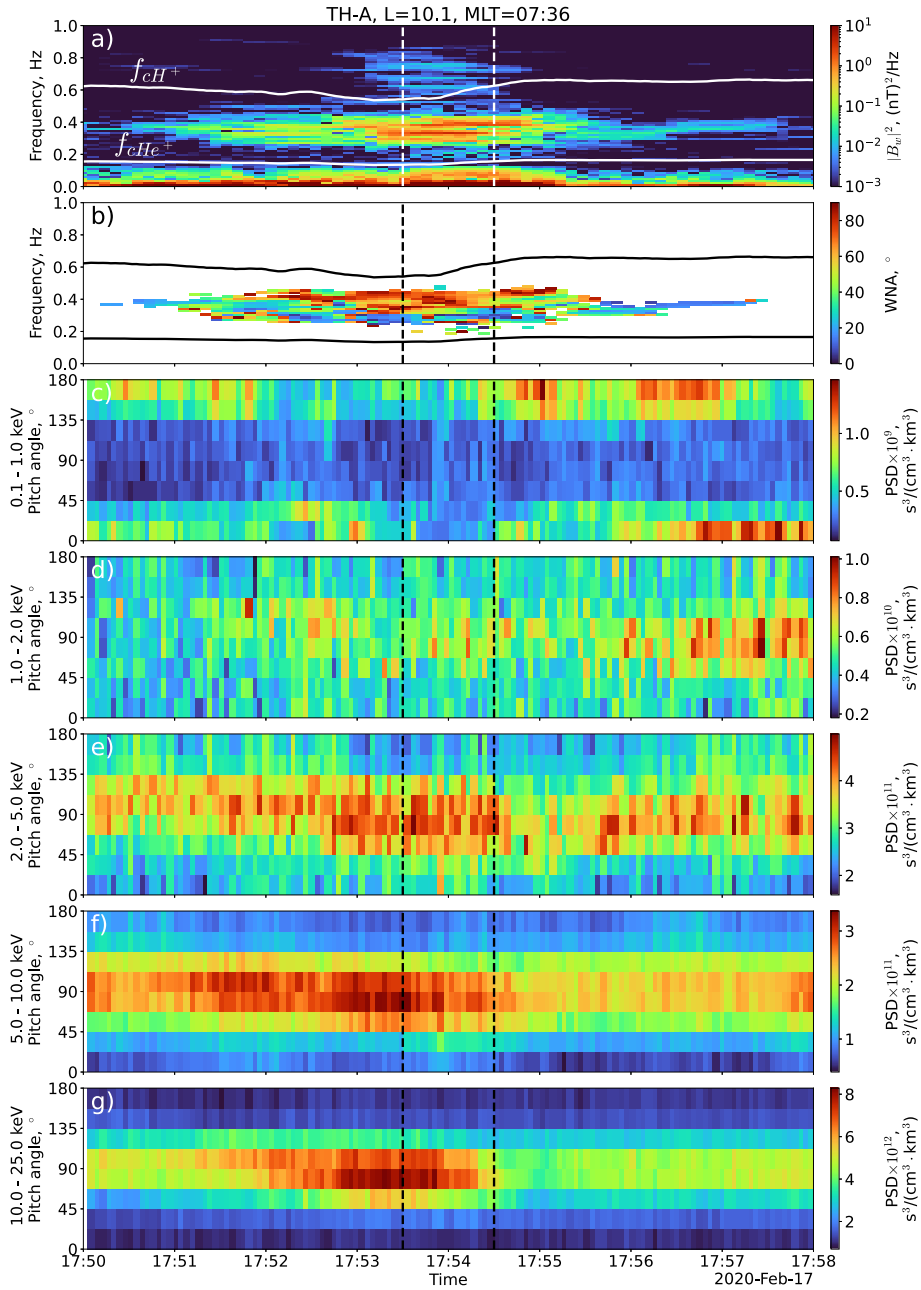

Figure 1. Observation of oblique, hydrogen-band EMIC waves by THEMIS-A spacecraft on 17 February 2020. (a) Wave magnetic field power spectrum, (b) wave normal angle; top and bottom lines represent hydrogen ion H^+ and helium ion He^+ cyclotron frequencies, respectively; vertical dashed lines mark the time interval that is used to average the ion phase space density for subsequent investigations of wave dispersion properties. For this and all other events, the wave polarization analysis has been conducted using an FFT window size of 1,280 samples (80s), with a step size of 128 samples (8s). (c–g) Ion pitch-angle distributions for different energy ranges as a function of time.

can reach 80° during this event. The ion beta is $\beta \sim 1.7$, typical for the inner plasma sheet edge/outer edge of the inner magnetosphere (Artemyev et al., 2018; Yue et al., 2017).

Figure 1 shows the field-aligned population of thermal ($\lesssim$1 keV) ions and hot (>2 keV), transversely anisotropic ion population. Both the flux and anisotropy of hot ions are large right around the moment of intense, very oblique EMIC waves. Such transversely anisotropic ions are likely responsible for EMIC wave generation (Chen

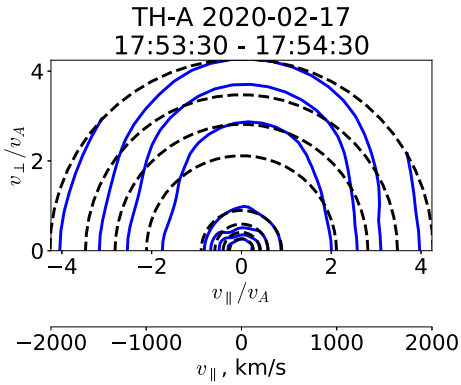

Figure 2. Snapshot of the ion distribution observed by THEMIS-A during the event on 17 February 2020 from Figure 1; ESA measurements are averaged over 17:53:30–17:54:30 UT, which are used to plot the contours of the ion phase space density (blue). For reference, the black dashed traces show contours of the particle energy.

et al., 2010, 2011; Yue et al., 2019), but instead of more typical field-aligned waves we observe very oblique waves. Therefore, certain features in the ion distribution significantly alter the generation mechanism. Most likely the thermal field-aligned ion population affects wave generation and moves the positive growth rate to high wave normal angles. To verify this assumption, we will combine the measured ion distribution and the linear dispersion solver.

Both the field-aligned thermal ion population and hot, transversely anisotropic population can be well seen in Figure 2, where we plot the 1-min averaged (around the time of the most intense wave spectrum) ion distribution in $(v_\parallel, v_\perp)$ plane. The velocities are normalized to the Alfvén velocity $v_A = B/\sqrt{4\pi n m_p}$, where n is the plasma density calculated from spacecraft potential, m_p is proton mass. Compared with the isotropic distribution (shown in black dashed curves), the observed distribution clearly shows a strong transverse anisotropy at $v_\perp > 0.5v_A$ and field-aligned anisotropy at $v_\perp < 0.25v_A$. This $(v_\parallel, v_\perp)$ distribution is then passed to the LEOPARD solver (Astfalk & Jenko, 2017) to calculate the wave dispersion relation, where we can determine the frequency–wave normal angle region of positive growth rate and compare this with observations of very oblique EMIC waves. Figure 3 shows results of LEOPARD calculations: the positive growth rate is indeed confined to very oblique wave normal angles, peaking at 74°, and to wave frequencies around $0.35 - 0.55 f_{cH+}$ (note throughout the paper we also use $\Omega_{ci} = 2\pi f_{cH+}$). These ranges of wave normal angles and frequencies are quite close to those observed by THEMIS (see Figure 1), which confirms that the ion distribution from Figure 2 can reliably reproduce the main wave properties. Note that there is no positive growth rate for field-aligned (or small wave normal angle) waves (not shown).

To reveal the ion distribution that is responsible for the generation of oblique EMIC waves, we compare two distributions: the first one is for the event with oblique EMIC waves from Figure 2, and the second one is for the typical event with field-aligned EMIC waves (this event is described below; see panel f) in Figure 5). To perform such a comparison, we normalize both distributions to isotropic spectrum $f_0(v)$ obtained from the field-aligned cut of distributions for each event (i.e., $f_0(v)$ does not depend on pitch-angle and is constructed as averages of pitch-angle bins at 11.25° and 168.75°). Thus, for each energy (semi-circles of constant $\sqrt{v_\parallel^2 + v_\perp^2}$), the transverse (field-aligned) anisotropy can be seen as a red (blue) area in near-perpendicular velocities. Figure 4 shows that in comparison with the field-aligned EMIC event, the oblique EMIC event is characterized by much stronger transverse anisotropy of the hot ion population and much smaller phase space density gradients around Landau resonance at thermal ion population energy range.

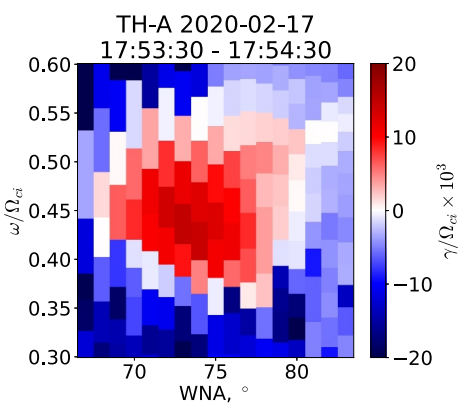

Figure 3. The estimated EMIC wave growth rate in the plane of wave normal angle and wave frequency. The growth rate is evaluated for proton-electron plasma with the ion distribution from Figure 2.

The main role of the thermal, field-aligned anisotropic population is to decrease Landau damping for oblique EMIC waves, and allow their generation. Indeed, in a typical case of field-aligned EMIC wave Figure 4b we observe quite strong gradient (blue region) of phase space density along the parallel velocity around the Landau resonance. This gradient is responsible for the damping of oblique waves, allowing only field-aligned waves to grow. In the event with oblique EMIC waves, the thermal field-aligned population decreases the gradient of the phase space density along the parallel velocity, which reduces the Landau damping and allows for wave generation via cyclotron resonance. Moreover, the same population reduces the total transverse anisotropy along the resonant curves, starting from the cyclotron resonant energies for field-aligned waves (not shown). Thus, in the event with oblique EMIC waves, the field-aligned thermal population prevents generation of field-aligned waves by reducing ion transverse anisotropy, while reduction of Landau damping opens a door for oblique wave generation. This feature of large transverse anisotropy of hot ions and lower energies of field-aligned thermal ions is typical for all events with oblique EMIC waves (see the next section).

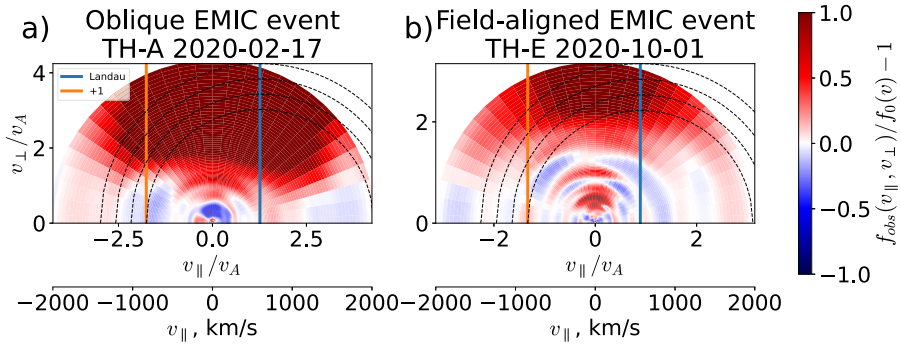

Figure 4. Comparison of ion distribution functions from (a) oblique and (b) field-aligned EMIC wave events. Distributions are normalized by the isotropic distribution $f_0(v)$ obtained as a average of parallel and antiparallel spectra: red regions show velocity domains with the transverse anisotropy, whereas blue regions shows domains with the field-aligned anisotropy. Blue and orange line show to Landau and first cyclotron resonant velocities for point (ω, k) corresponding to maximum growth rate from the hot plasma dispersion. Black dashed lines show contours of constant energy in the wave frame (Lyons & Williams, 1984).

3.2. Comparison of Ion Distributions During Field-Aligned and Oblique EMIC Events

Figures 5b–5e shows four more examples of THEMIS observed very oblique EMIC waves in the dawn flank. All these events share similar properties of the event discussed in Section 3.1:

- Waves are proton band EMIC waves with clear maximum of the wave intensity around [0.3, 0.5] of local proton cyclotron frequency and with wave normal angles typically exceeding 60° (left panels).
- Ion distribution functions (middle panels) observed around the oblique EMIC wave burst include a very anisotropic hot (a few keVs) ion population ($\beta_\perp/\beta_\parallel > 3$) and a field-aligned anisotropic thermal ($\leq$1 keV) ion population. The latter can lead to strong cyclotron damping of field-aligned EMIC waves.
- Combining the measured ion distribution and the linear dispersion solver, LEOPARD, we show positive growth rates for very oblique EMIC waves (right panels), as well as damping for the field-aligned waves (not shown). Therefore, the most important condition for very oblique EMIC wave generation is likely the combination of transversely anisotropic hot ions (providing wave growth via cyclotron resonance) and field-aligned thermal ions (providing cyclotron damping of small wave normal angle waves).

To verify the importance of the thermal field-aligned population for very oblique EMIC wave growth, we further selected a typical field-aligned EMIC wave event observed by THEMIS in the dusk flank. As shown in Figure 5f, in the absence of field-aligned thermal ions, the field-aligned waves can be generated via cyclotron resonance with transversely anisotropic hot ions. Moreover, in the absence of the field-aligned population, the anisotropy of the entire ion distribution is mainly determined by the anisotropy of hot ions, which does not need to be as large as in events with oblique waves in order to generate field-aligned waves. As a result, in the event from Figure 5f the hot ion anisotropy, $\beta_\perp/\beta_\parallel = 1.3$, is sufficient to generate field-aligned EMIC waves, but insufficient to generate oblique waves (the growth rate of oblique waves is negative for this event; not shown).

4. Discussion and Conclusions

In this study we analyze several events with THEMIS observations of very oblique EMIC waves around the equator. During these events, the observed ion distributions consist of a highly transversely anisotropic ($\beta_\perp/\beta_\parallel \sim 4$, >2 keV) hot ion population and a field-aligned anisotropic thermal ion population ($\beta_\perp/\beta_\parallel \sim 0.3$, <1 keV). It is this field-aligned thermal ion population that prohibits the generation of field-aligned EMIC waves: the cyclotron resonant energy of waves with small wave normal angles is ~1 keV, where the transverse anisotropy is insufficient to drive these waves. Therefore, such thermal (<1 keV) field-aligned ion population play a key role in producing very oblique EMIC waves, which are often observed on the dawn flank. The energy range and field-aligned anisotropy of this population suggest that these are likely ionospheric outflow ions (see statistics of ion pitch-angle distributions in Artemyev et al., 2018; Yue et al., 2017). Overlapping of such outflow, probably enhanced at the dawn flank due to strong plasma sheet electron precipitation driven by whistler-mode waves (Ni

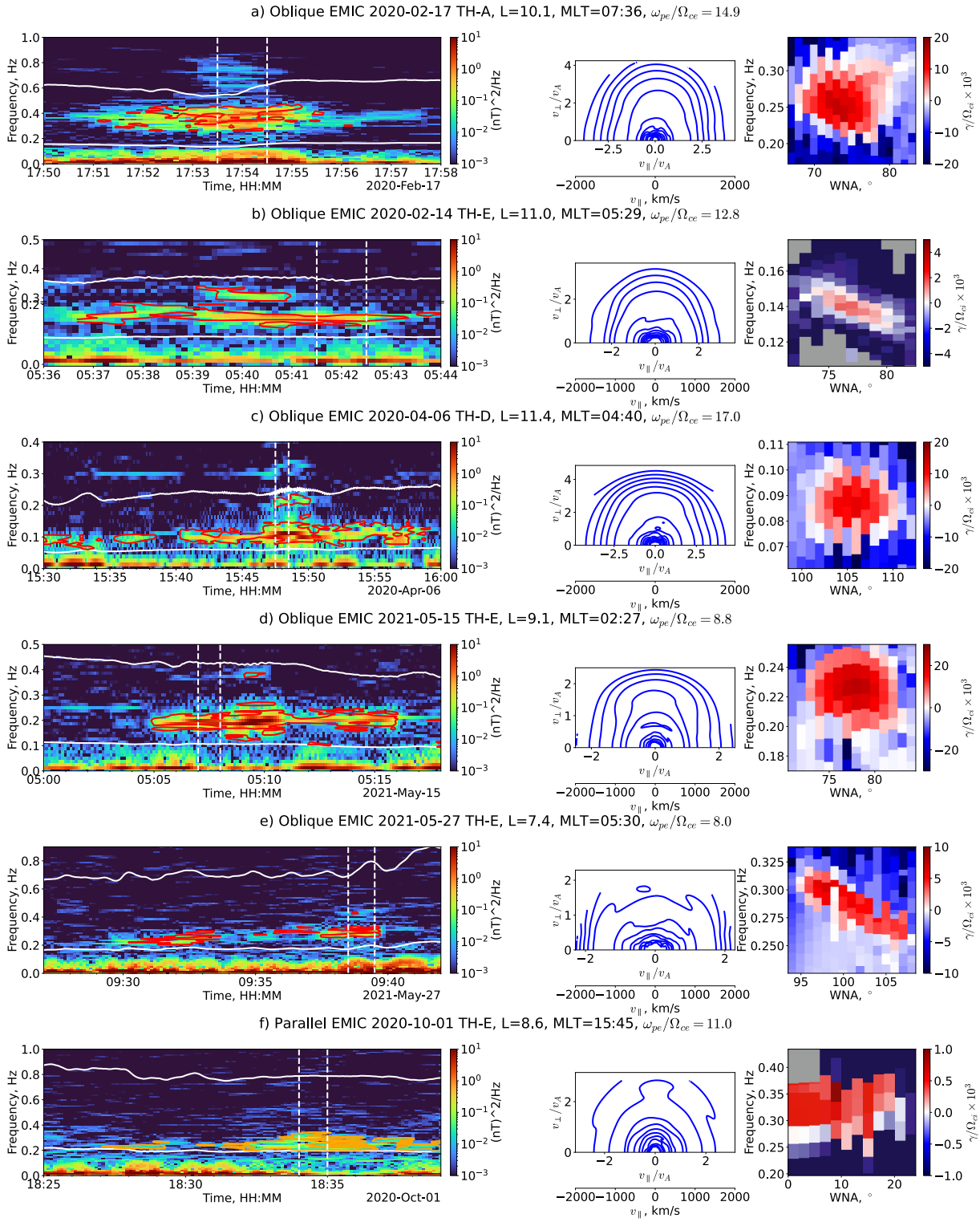

Figure 5. Wave magnetic field power spectrum (left column), ion distribution (center column), and wave growth rate (right column) for oblique (a–e) and field-aligned (f) EMIC wave events. In the wave power spectra: for oblique EMIC waves, red contours show the domain where wave normal angle >60°, whereas for field-aligned EMIC wave event orange contours show the domain where wave normal angle <20°; the two horizontal white lines mark hydrogen and helium ion gyrofrequencies from top to bottom. During the 14 February 2020 event (b), part of the wave spectrum has been cut to remove the spin tones that obscure the waves.

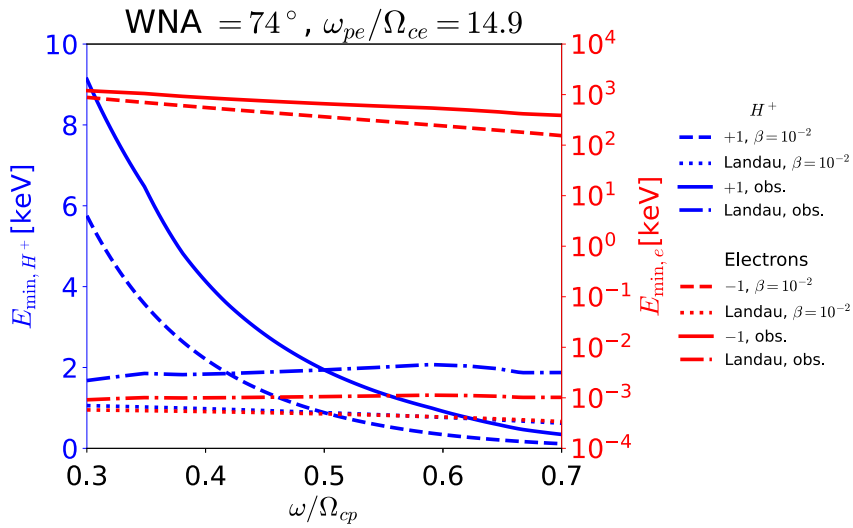

Figure 6. Figure legend updated to include description for both proton and electron resonant energies. Minimum resonant energies for protons (blue, linear scale) and electrons (red, logarithmic scale) in Landau resonance and first cyclotron resonance (… "+1" for protons, "−1" for electrons). Dashed and dotted lines are calculated using generic bi-Maxwellian distributions (with $\beta = 10^{-2}$), whereas solid and dot-dashed lines are based on the dispersion relation of EMIC waves for the first event (Figure 5a).

et al., 2016; Thorne et al., 2010), and the hot ion population, likely drifted from the dusk flank after being injected from the plasmasheet (e.g., Birn et al., 1997; Gabrielse et al., 2014; Ukhorskiy et al., 2018), creates favorable conditions for the generation of very oblique EMIC waves. This further implies that very oblique waves are likely a result of magnetosphere-ionosphere coupling, in contrast to the more typical field-aligned waves generated in the dusk flank due to plasmasheet injections or on the dayside due to magnetosphere compression by the solar wind (Jun et al., 2019, 2021; Yue et al., 2019).

In addition to the possible resonant interactions between oblique EMIC waves and magnetospheric particles, as discussed in the introduction, a new resonant mechanism has been proposed recently that makes oblique EMIC waves potentially more important. It has been shown by Hanzelka et al. (2024) that very oblique and sufficiently intense EMIC waves may resonate with energetic electrons via the so-called fractional (or subharmonic) resonances (Lewak & Chen, 1969; Smirnov & Frank-Kamenestkiĭ, 1968). In contrast to cyclotron resonances with integer resonant numbers, the factional resonance is a purely nonlinear effect providing electron scattering in resonances with fractional numbers (Terasawa & Matsukiyo, 2012), which reduces the electron energy in resonance with EMIC waves to sub-relativistic values (Hanzelka et al., 2024). THEMIS observations of very oblique EMIC waves and the proposed formation mechanism of these waves suggest that sub-relativistic electron precipitation on the dawn side (see statistics of such precipitation in Tsai et al., 2023) may be partly driven by EMIC waves, not exclusively by whistler-mode waves.

Figure 6 shows the energies of electrons and ions in resonance with very oblique EMIC waves (we use a wave normal angle of 74° and plot resonant energies as a function of wave frequency for typical plasma frequencies as from Figure 5). Note that the electron resonant energies for fractional resonances fall between the regions bounded by the first cyclotron resonance, $n = -1$, and Landau resonance, $n = 0$ (Hanzelka et al., 2023). Comparing the results for the cold plasma dispersion $(\beta = 10^{-2})$ and for the observed hot plasma with $\beta \approx 1.7$, we can see a higher resonant energy for the hot plasma case due to a decrease of the wave number at a fixed frequency (Silin et al., 2011). Cyclotron and Landau resonant energies for protons are within [1,10]keV for $\omega/\Omega_{cp} < 0.5$, where most of wave power is observed (see Figure 5a). This energy range allows oblique EMIC waves to heat thermal ($\sim$1 keV) ions and scatter ring current ($\sim$10 keV) ions into the loss cone (note that these resonant energies are calculated at the equator, which will increase in the off-equatorial region). The range of resonant energies for electrons, on the other hand, is much wider: from $\sim$1 eV in Landau resonance to 1 MeV in cyclotron resonance. The fractional resonances with a resonance number $\in [0, 1]$ will fill this gap and allow EMIC

waves to also scatter hundreds of keV electrons. This is likely the most interesting and potentially important implication of very oblique waves.

To conclude, using THEMIS observations in the inner magnetosphere, we have investigated the generation mechanism of very oblique EMIC waves. Six typical events of such waves are observed at the dawn flank, in contrast to the more common field-aligned waves observed at the dusk and noon sectors. Very oblique EMIC waves are usually accompanied by ion distributions consisting of two main populations (except for the cold plasma population contributing to the total density). (a) For field-aligned waves, which only resonate with ions through the cyclotron resonance, the presence of a thermal ion population, at ≤1 keV, with field-line anisotropy can effectively decrease the fundamental cyclotron resonance growth rate (i.e., increase wave damping/decrease wave growth). In contrast, oblique waves can resonate with ions through cyclotron and Landau resonance, and Landau damping of these waves is determined by the slope of ion distributions along the parallel velocity. The presence of a thermal ion population, at ≤1 keV, with field-line anisotropy can reduce this slope (form the plateau) and thus reduce the Landau damping of oblique waves. This population shares the same properties of ionospheric outflow as reported previously for the inner magnetosphere (e.g., Yue et al., 2017). (b) The hot ion population, at >5 keV, with a strong transverse anisotropy ($\beta_\perp/\beta_\parallel \sim 4$) providing the cyclotron resonant growth of oblique EMIC waves with wave normal angles exceeding 60°. These observations underline the importance of magnetosphere-ionosphere coupling in producing very oblique EMIC waves.

Data Availability Statement

THEMIS data is available at http://themis.ssl.berkeley.edu. Data access and processing was performed using SPEDAS V4.1 and its Python-based implementation, see Angelopoulos et al. (2019) and (Grimes et al., 2022).

Acknowledgments
We acknowledge the support of NASA contract NAS5-02099 for the use of data from the THEMIS Mission, specifically K. H.Glassmeier, U. Auster and W. Baumjohann for the use of FGM data (provided under the lead of the Technical University of Braunschweig and with financial support through the German Ministry for Economy and Technology and the German Center for Aviation and Space (DLR) under contract 50 OC 0302). Work of D.S.T., X.-J. Z., and A.V.A. are supported by NSF Grant 2329897, and NASA Grants 80NSSC23K0403, 80NSSC23K0108, 80NSSC24K0138, 80NSSC24K0558. X. A. is supported by NSF Grant 2108582 and NASA Grant 80NSSC20K0917.

References

Angelopoulos, V. (2008). The THEMIS mission. *Space Science Reviews*, *141*(1–4), 5–34. https://doi.org/10.1007/s11214-008-9336-1

Angelopoulos, V., Cruce, P., Drozdov, A., Grimes, E. W., Hatzigeorgiu, N., King, D. A., et al. (2019). The space physics environment data analysis system (SPEDAS). *Space Science Reviews*, *215*(1), 9. https://doi.org/10.1007/s11214-018-0576-4

Artemyev, A. V., Angelopoulos, V., Runov, A., & Zhang, X. J. (2020). Ionospheric outflow during the substorm growth phase: THEMIS observations of oxygen ions at the plasma sheet boundary. *Journal of Geophysical Research (Space Physics)*, *125*(7), e27612. https://doi.org/10.1029/2019JA027612

Artemyev, A. V., & Mourenas, D. (2020). On whistler mode wave relation to electron field-aligned plateau populations. *Journal of Geophysical Research (Space Physics)*, *125*(3), e27735. https://doi.org/10.1029/2019JA027735

Artemyev, A. V., Zhang, X. J., Angelopoulos, V., Runov, A., Spence, H. E., & Larsen, B. A. (2018). Plasma anisotropies and currents in the near-Earth plasma sheet and inner magnetosphere. *Journal of Geophysical Research (Space Physics)*, *123*(7), 5625–5639. https://doi.org/10.1029/2018JA025232

Astfalk, P., & Jenko, F. (2017). Leopard: A grid-based dispersion relation solver for arbitrary gyrotropic distributions. *Journal of Geophysical Research (Space Physics)*, *122*(1), 89–101. https://doi.org/10.1002/2016JA023522

Auster, H. U., Glassmeier, K. H., Magnes, W., Aydogar, O., Baumjohann, W., Constantinescu, D., et al. (2008). The THEMIS fluxgate magnetometer. *Space Science Reviews*, *141*(1–4), 235–264. https://doi.org/10.1007/s11214-008-9365-9

Birn, J., Thomsen, M. F., Borovsky, J. E., Reeves, G. D., McComas, D. J., Belian, R. D., & Hesse, M. (1997). Substorm ion injections: Geosynchronous observations and test particle orbits in three-dimensional dynamic MHD fields. *Journal of Geophysical Research*, *102*, 2325–2342. https://doi.org/10.1029/96JA03032

Blum, L. W., Artemyev, A., Agapitov, O., Mourenas, D., Boardsen, S., & Schiller, Q. (2019). EMIC wave-driven bounce resonance scattering of energetic electrons in the inner magnetosphere. *Journal of Geophysical Research (Space Physics)*, *124*(4), 2484–2496. https://doi.org/10.1029/2018JA026427

Bonnell, J. W., Mozer, F. S., Delory, G. T., Hull, A. J., Ergun, R. E., Cully, C. M., et al. (2008). The electric field instrument (EFI) for THEMIS. *Space Science Reviews*, *141*(1–4), 303–341. https://doi.org/10.1007/s11214-008-9469-2

Chen, L., Thorne, R. M., & Bortnik, J. (2011). The controlling effect of ion temperature on EMIC wave excitation and scattering. *Geophysical Research Letters*, *38*(16), L16109. https://doi.org/10.1029/2011GL048653

Chen, L., Thorne, R. M., Jordanova, V. K., Wang, C.-P., Gkioulidou, M., Lyons, L., & Horne, R. B. (2010). Global simulation of EMIC wave excitation during the 21 April 2001 storm from coupled RCM-RAM-HOTRAY modeling. *Journal of Geophysical Research (Space Physics)*, *115*(A7), A07209. https://doi.org/10.1029/2009JA015075

Cornwall, J. M., Coroniti, F. V., & Thorne, R. M. (1970). Turbulent loss of ring current protons. *Journal of Geophysical Research*, *75*(25), 4699–4709. https://doi.org/10.1029/JA075i025p04699

Cornwall, J. M., Coroniti, F. V., & Thorne, R. M. (1971). Unified theory of SAR arc formation at the plasmapause. *Journal of Geophysical Research*, *76*(19), 4428–4445. https://doi.org/10.1029/JA076i019p04428

Cornwall, J. M., & Schulz, M. (1971). Electromagnetic ion-cyclotron instabilities in multicomponent magnetospheric plasmas. *Journal of Geophysical Research*, *76*(31), 7791–7796. https://doi.org/10.1029/JA076i031p07791

de Soria-Santacruz, M., Spasojevic, M., & Chen, L. (2013). EMIC waves growth and guiding in the presence of cold plasma density irregularities. *Geophysical Research Letters*, *40*(10), 1940–1944. https://doi.org/10.1002/grl.50484

Fraser, B. J., & Nguyen, T. S. (2001). Is the plasmapause a preferred source region of electromagnetic ion cyclotron waves in the magnetosphere? *Journal of Atmospheric and Solar-Terrestrial Physics*, *63*(11), 1225–1247. https://doi.org/10.1016/S1364-6826(00)00225-X

Gabrielse, C., Angelopoulos, V., Runov, A., & Turner, D. L. (2014). Statistical characteristics of particle injections throughout the equatorial magnetotail. *Journal of Geophysical Research*, *119*(4), 2512–2535. https://doi.org/10.1002/2013JA019638

Grimes, E. W., Harter, B., Hatzigeorgiu, N., Drozdov, A., Lewis, J. W., Angelopoulos, V., et al. (2022). The space physics environment data analysis system in python. *Frontiers in Astronomy and Space Sciences*, *9*, 1020815. https://doi.org/10.3389/fspas.2022.1020815

Hanzelka, M., Li, W., & Ma, Q. (2023). Parametric analysis of pitch angle scattering and losses of relativistic electrons by oblique EMIC waves. *Frontiers in Astronomy and Space Sciences*, *10*, 1163515. https://doi.org/10.3389/fspas.2023.1163515

Hanzelka, M., Li, W., Qin, M., Capannolo, L., Shen, X., Ma, Q., et al. (2024). Sub-MeV electron precipitation driven by EMIC waves through nonlinear fractional resonances. *Geophysical Research Letters*, *51*(8), e2023GL107355. https://doi.org/10.1029/2023GL107355

Jun, C.-W., Miyoshi, Y., Kurita, S., Yue, C., Bortnik, J., Lyons, L., et al. (2021). The characteristics of EMIC waves in the magnetosphere based on the van allen probes and Arase observations. *Journal of Geophysical Research (Space Physics)*, *126*(6), e29001. https://doi.org/10.1029/2020JA029001

Jun, C. W., Yue, C., Bortnik, J., Lyons, L. R., Nishimura, Y., & Kletzing, C. (2019). EMIC wave properties associated with and without injections in the inner magnetosphere. *Journal of Geophysical Research (Space Physics)*, *124*(3), 2029–2045. https://doi.org/10.1029/2018JA026279

Khazanov, G. V., & Gamayunov, K. V. (2007). Effect of electromagnetic ion cyclotron wave normal angle distribution on relativistic electron scattering in outer radiation belt. *Journal of Geophysical Research (Space Physics)*, *112*(A10), A10209. https://doi.org/10.1029/2007JA012282

Kim, H., Schiller, Q., Engebretson, M. J., Noh, S., Kuzichev, I., Lanzerotti, L. J., et al. (2021). Observations of particle loss due to injection associated electromagnetic ion cyclotron waves. *Journal of Geophysical Research (Space Physics)*, *126*(2), e28503. https://doi.org/10.1029/2020JA028503

Kitamura, N., Kitahara, M., Shoji, M., Miyoshi, Y., Hasegawa, H., Nakamura, S., et al. (2018). Direct measurements of two-way wave-particle energy transfer in a collisionless space plasma. *Science*, *361*(6406), 1000–1003. https://doi.org/10.1126/science.aap8730

Lee, D.-Y., Shin, D.-K., & Choi, C.-R. (2018). Effects of oblique wave normal angle and noncircular polarization of electromagnetic ion cyclotron waves on the pitch angle scattering of relativistic electrons. *Journal of Geophysical Research (Space Physics)*, *123*(6), 4556–4573. https://doi.org/10.1029/2018JA025342

Lewak, G. J., & Chen, C. S. (1969). Higher order resonances in a plasma. *Journal of Plasma Physics*, *3*(3), 481–497. https://doi.org/10.1017/S0022377800004554

Li, W., Mourenas, D., Artemyev, A. V., Bortnik, J., Thorne, R. M., Kletzing, C. A., et al. (2016). Unraveling the excitation mechanisms of highly oblique lower band chorus waves. *Geophysical Research Letters*, *43*(17), 8867–8875. https://doi.org/10.1002/2016GL070386

Liu, Y. H., Fraser, B. J., & Menk, F. W. (2013). EMIC waves observed by Cluster near the plasmapause. *Journal of Geophysical Research (Space Physics)*, *118*(9), 5603–5615. https://doi.org/10.1002/jgra.50486

Lyons, L. R., & Williams, D. J. (1984). In L. R. Lyons & D. J. Williams (Eds.), *Quantitative aspects of magnetospheric physics* (pp. 133–142). Springer.

Ma, Q., Li, W., Yue, C., Thorne, R. M., Bortnik, J., Kletzing, C. A., et al. (2019). Ion heating by electromagnetic ion cyclotron waves and magnetosonic waves in the Earth's inner magnetosphere. *Geophysical Research Letters*, *46*(12), 6258–6267. https://doi.org/10.1029/2019GL083513

McFadden, J. P., Carlson, C. W., Larson, D., Ludlam, M., Abiad, R., Elliott, B., et al. (2008). The THEMIS ESA plasma instrument and in-flight calibration. *Space Science Reviews*, *141*(1–4), 277–302. https://doi.org/10.1007/s11214-008-9440-2

Means, J. D. (1972). Use of the three-dimensional covariance matrix in analyzing the polarization properties of plane waves. *Journal of Geophysical Research*, *77*(28), 5551–5559. https://doi.org/10.1029/JA077i028p05551

Min, K., Liu, K., Bonnell, J. W., Breneman, A. W., Denton, R. E., Funsten, H. O., et al. (2015). Study of EMIC wave excitation using direct ion measurements. *Journal of Geophysical Research (Space Physics)*, *120*(4), 2702–2719. https://doi.org/10.1002/2014JA020717

Mourenas, D., Artemyev, A. V., Agapitov, O. V., Krasnoselskikh, V., & Mozer, F. S. (2015). Very oblique whistler generation by low-energy electron streams. *Journal of Geophysical Research*, *120*(5), 3665–3683. https://doi.org/10.1002/2015JA021135

Ni, B., Thorne, R. M., Zhang, X., Bortnik, J., Pu, Z., Xie, L., et al. (2016). Origins of the Earth's diffuse auroral precipitation. *Space Science Reviews*, *200*(1–4), 205–259. https://doi.org/10.1007/s11214-016-0234-7

Nishimura, Y., Bortnik, J., Li, W., Thorne, R. M., Ni, B., Lyons, L. R., et al. (2013). Structures of dayside whistler-mode waves deduced from conjugate diffuse aurora. *Journal of Geophysical Research (Space Physics)*, *118*(2), 664–673. https://doi.org/10.1029/2012JA018242

Omura, Y., Ashour-Abdalla, M., Gendrin, R., & Quest, K. (1985). Heating of thermal helium in the equatorial magnetosphere: A simulation study. *Journal of Geophysical Research*, *90*(A9), 8281–8292. https://doi.org/10.1029/JA090iA09p08281

Rauch, J. L., & Roux, A. (1982). Ray tracing of ULF waves in a multicomponent magnetospheric plasma: Consequences for the generation mechanism of ion cyclotron waves. *Journal of Geophysical Research*, *87*(A10), 8191–8198. https://doi.org/10.1029/JA087iA10p08191

Silin, I., Mann, I. R., Sydora, R. D., Summers, D., & Mace, R. L. (2011). Warm plasma effects on electromagnetic ion cyclotron wave MeV electron interactions in the magnetosphere. *Journal of Geophysical Research (Space Physics)*, *116*(A5), A05215. https://doi.org/10.1029/2010JA016398

Smirnov, Y. N., & Frank-Kamenestkiĭ, D. A. (1968). Nonlinearity and parametric resonance in a plasma. *Soviet Journal of Experimental and Theoretical Physics*, *26*, 627.

Terasawa, T., & Matsukiyo, S. (2012). Cyclotron resonant interactions in cosmic particle accelerators. *Space Science Reviews*, *173*(1–4), 623–640. https://doi.org/10.1007/s11214-012-9878-0

Thorne, R. M., & Horne, R. B. (1992). The contribution of ion-cyclotron waves to electron heating and SAR-arc excitation near the storm-time plasmapause. *Geophysical Research Letters*, *19*(4), 417–420. https://doi.org/10.1029/92GL00089

Thorne, R. M., & Horne, R. B. (1997). Modulation of electromagnetic ion cyclotron instability due to interaction with ring current O+ during magnetic storms. *Journal of Geophysical Research*, *102*(A7), 14155–14164. https://doi.org/10.1029/96JA04019

Thorne, R. M., Ni, B., Tao, X., Horne, R. B., & Meredith, N. P. (2010). Scattering by chorus waves as the dominant cause of diffuse auroral precipitation. *Nature*, *467*(7318), 943–946. https://doi.org/10.1038/nature09467

Tsai, E., Artemyev, A., Angelopoulos, V., & Zhang, X.-J. (2023). Investigating whistler-mode wave intensity along field lines using electron precipitation measurements. *Journal of Geophysical Research (Space Physics)*, *128*(8), e2023JA031578. https://doi.org/10.1029/2023JA031578

Ukhorskiy, A. Y., Sorathia, K. A., Merkin, V. G., Sitnov, M. I., Mitchell, D. G., & Gkioulidou, M. (2018). Ion trapping and acceleration at dipolarization fronts: High-resolution MHD and test-particle simulations. *Journal of Geophysical Research (Space Physics)*, *123*(7), 5580–5589. https://doi.org/10.1029/2018JA025370

Usanova, M. E. (2021). Energy exchange between electromagnetic ion cyclotron (EMIC) waves and thermal plasma: From theory to observations. *Frontiers in Astronomy and Space Sciences*, *8*, 150. https://doi.org/10.3389/fspas.2021.744344

Usanova, M. E., Mann, I. R., & Darrouzet, F. (2016). EMIC waves in the inner magnetosphere. *Washington DC American Geophysical Union Geophysical Monograph Series*, *216*, 65–78. https://doi.org/10.1002/9781119055006.ch5

Wang, B., Li, P., Huang, J., & Zhang, B. (2019). Nonlinear Landau resonance between EMIC waves and cold electrons in the inner magnetosphere. *Physics of Plasmas*, *26*(4), 042903. https://doi.org/10.1063/1.5088374

Wang, Q., Fu, S., Ni, B., Cao, X., Gu, X., & Huang, H. (2018). Bounce resonance scattering of ring current electrons by H+ band EMIC waves. *Physics of Plasmas*, *25*(8), 082903. https://doi.org/10.1063/1.5043522

Yue, C., Bortnik, J., Thorne, R. M., Ma, Q., An, X., Chappell, C. R., et al. (2017). The characteristic pitch angle distributions of 1 ev to 600 kev protons near the equator based on van Allen probes observations. *Journal of Geophysical Research*, *122*(9), 9464–9473. https://doi.org/10.1002/2017JA024421

Yue, C., Jun, C.-W., Bortnik, J., An, X., Ma, Q., Reeves, G. D., et al. (2019). The relationship between EMIC wave properties and proton distributions based on van allen probes observations. *Geophysical Research Letters*, *46*(8), 4070–4078. https://doi.org/10.1029/2019GL082633